Histol Histopathol (2019) 34: 479-490

http://www.hh.um.es

Histology and Histopathology

From Cell Biology to Tissue Engineering

Membrane trafficking and exocytosis are upregulated in port wine stain blood vessels

Rong Yin[1,2,9], Shawn J. Rice[3], Jinwei Wang[1,8], Lin Gao[5], Joseph Tsai[1], Radean T. Anvari[1], Fang Zhou[1,8], Xin Liu[3], Gang Wang[5], Yuxin Tang[8], Martin C. Mihm Jr[6], Chandra P. Belani[3,4], Dong-bao Chen[10], J. Stuart Nelson[1,7] and Wenbin Tan[1,2]

[1]Department of Surgery, Beckman Laser Institute and Medical Clinic, University of California, Irvine, California, [2]Department of Cell Biology and Anatomy, University of South Carolina School of Medicine, Columbia, South Carolina, [3]Penn State Cancer Institute, [4]Department of Medicine, Penn State College of Medicine, Hershey, USA, [5]Department of Dermatology, Xijing Hospital, Xi'an, China, [6]Department of Dermatology, Brigham and Women's Hospital, Harvard Medical School, Boston, Massachusetts, [7]Department of Biomedical Engineering, University of California, Irvine, California, USA, [8]Department of Urology, the Xiangya 3rd Hospital, Xiangya School of Medicine, Central South University, Changsha, Hunan, [9]Department of Dermatology, the Second Hospital of Shanxi Medical University, Taiyuan, China and [10]Department of Obstetrics and Gynecology, University of California, Irvine, California, USA

Summary. Introduction. Port wine stain (PWS) is characterized as a progressive dilatation of immature venule-like vasculatures which result from differentiation-impaired endothelial cells. In this study, we aimed to identify the major biological pathways accounting for the pathogenesis of PWS.

Methods. Sequential windowed acquisition of all theoretical fragment ion mass spectra (SWATH-MS) was used to identify differentially expressed proteins in PWS lesions, followed by confirmative studies with immunohistochemistry, immunoblot and transmission electron microscopy (TEM).

Results. 107 out of 299 identified proteins showed differential expressions in PWS lesions as compared to normal skin, mainly involving the functions of biosynthesis, membrane trafficking, cytoskeleton and cell adhesion/migration. The confirmative studies showed that expressions of membrane trafficking/exocytosis related proteins such as VAT1, IQGAP1, HSC70, clathrin, perlecan, spectrin α1 and GDIR1 were significantly increased in PWS blood vessels as compared to normal ones. Furthermore, TEM studies showed there is a significant upregulation of extracellular vesicle exocytosis from PWS blood vessels as compared to control.

Conclusions. The biological process of membrane trafficking and exocytosis is enhanced in PWS blood vessels. Our results imply that the extracellular vesicles released by lesional endothelial cells may act as potential intercellular signaling mediators to contribute to the pathogenesis of PWS.

Key words: Port wine stain, Vascular malformations, Endothelial cells, Extracellular vesicle, Exocytosis, SWATH-MS

Introduction

Port wine stain (PWS) is a congenital vascular malformation resulting from differentiation-impaired endothelial cells (ECs) in human skin with a progressive dilatation of immature venule-like vasculatures (Tan et al., 2017). The prevalence is estimated at 3-5 children per 1,000 live births (Pratt, 1953; Jacobs and Walton, 1976). PWS initially appears as flat red macules in childhood; lesions tend to darken progressively to purple with soft tissue hypertrophy and, by middle age, they often become raised as a result of the development of vascular nodules which are susceptible to spontaneous

Offprint requests to: Wenbin Tan, Department of Cell Biology and Anatomy, University of South Carolina School of Medicine, Columbia, South Carolina 29209, USA; Department of Surgery, Beckman Laser Institute and Medical Clinic, University of California, Irvine, California 92617, USA. e-mail: wenbin.tan@uscmed.sc.edu or wenbint@uci.edu

DOI: 10.14670/HH-18-051

bleeding or hemorrhage (Lever and Schaumburg-Lever, 1990; Geronemus and Ashinoff, 1991). PWS is a significant clinical problem that results in loss of self-esteem since most malformations occur on the face (Kalick, 1978; Heller et al., 1985; Malm and Carlberg, 1988). The pulsed dye laser (PDL) is the treatment of choice for PWS but the regrowth of pathologic blood vessels post-PDL treatment is a major clinical barrier that needs to be overcome (Tan et al., 2012; Gao et al., 2014). The pathogenesis of PWS remains incompletely understood. Recent studies have suggested that the sporadic somatic mutation of guanine nucleotide-binding protein, G alpha subunit q (*gnaq*) (c.548G>A), is linked to PWS (Shirley et al., 2013; Lian et al., 2014). The *gnaq* (c.548G>A) is primarily present in PWS blood vessels (Couto et al., 2016; Tan et al., 2016a). In addition, PWS have sustained activation of mitogen-activated protein kinases in the infantile stage and, particularly, activation of PKCα and PI3K pathways in hypertrophic and nodular lesions (Tan et al., 2014; Yin et al., 2017). We have recently characterized that PWS blood vessels are immature venule-like vasculatures with aberrant expressions of stem cell markers CD133 and CD166, venous marker EphB1 and arterial marker Ephrin B2 (EfnB2). The disruption of normal EC-EC interactions by co-existence of EphB1 and EfnB2 contributes to progressive dilatation of PWS vasculatures (Tan et al., 2017).

In this study, we aimed to identify differentially expressed (DE) proteins in PWS lesions as compared to normal skin using a proteomics approach, namely sequential windowed acquisition of all theoretical fragment ion mass spectra (SWATH-MS). We then performed a further investigation to determine their expression patterns and cellular localizations in PWS hypertrophic lesions and nodules as compared to control. We found that PWS blood vessels have increased expressions of cell membrane trafficking/exocytosis related molecules and that the exocytosis of extracellular vesicles (EVs) is enhanced in PWS blood vessels.

Materials and methods

Patients and tissue samples

This study was approved by the Institutional Review Board at the University of California, Irvine (UCI) (#2013-9396) and Xijing Hospital. A total of 21 PWS biopsies and 6 adjacent normal skin samples were obtained from 13 subjects and de-identified for this study. The clinical characteristics of the subjects and biopsy samples have been described previously (Tan et al., 2014; Yin et al., 2017).

SWATH-MS

The formalin-fixed paraffin-embedded (FFPE) sections were used for SWATH-MS. There were two groups of specimens, e.g., control (n=3) and PWS (n=6). The protocols of protein extraction from FFPE sections and peptide library preparation have been previously reported (Ostasiewicz et al., 2010). All samples were duplicated during the mass spectrometry studies. Mass spectra were acquired on an AB Sciex 5600+ triple TOF mass spectrometer (AB Sciex, Framingham, MA) in data independent acquisition (DIA) mode. Each SWATH cycle included an MS1 scan and 32 equal SWATH window scans covering the entire MS1 scan range (400-1200 m/z). The DIA files were analyzed using DIA-Umpire according to a previously published protocol with default setting (Deutsch et al., 2010; Tsou et al., 2015). The quantification and re-extraction module of DIA-Umpire was used to quantify proteins. iBAQ and MS2 (Top 6 peptides) protein quantities were analyzed using the Perseus software package with a Student's T-Test (Tyanova et al., 2016).

Immunoblot and Immunohistochemistry (IHC)

The procedures of immunoblot and immunohistochemistry (IHC) and on PWS and control tissues followed the protocols in our previous studies (Tan et al., 2014, 2016a,b; Gao et al., 2017; Yin et al., 2017). The fresh skin biopsy samples were homogenized in radio-immunoprecipitation assay (RIPA) buffer (25 mM Tris, 150 mM NaCl, 0.1% SDS, 0.5% sodium deoxycholate, 1% NP-40) containing cocktail proteinase inhibitors. The protein was quantified. For immunoblot, 5-10 μg of total proteins was loaded per lane. The primary antibodies including IQ motif containing GTPase activating protein 1 (IQGAP1), vesicle amine transport 1 (VAT1), spectrin 1α, clathrin, Rho GDP dissociation inhibitor (GDI) alpha (GDIR1), heat shock cognate protein 70 (HSC70), perlecan, annexin A1 (anx1), collagen 6A1 (col6A1), col6A3, vitamin D binding protein (VDBP) and glyceraldehyde 3-phosphate dehydrogenase (GAPDH) were from Santa Cruz Biotechnology. The dilution for all primary antibodies was 1:3000 and GAPDH was used as the loading control. For IHC, approximately 6 μm thick paraffin sections were cut and antigen retrieval was performed in 10 mM sodium citrate buffer (pH 6.0) at 97°C for 3 hrs. Sections were then incubated in a humidified chamber overnight at 4°C with the following primary antibodies: anti-IQGAP1 (1:50), anti-spectrin 1α (1:50), anti-clathrin (1:50), anti-GDIR1 (1:100) and anti-HSC70 (1:200). Biotinylated anti-mouse secondary antibodies were incubated with the sections for 2 hrs. at room temperature after the primary antibodies' reaction. An indirect biotin avidin diaminobenzidine (DAB) system (Dako, Glostrup, Denmark) was used for detection.

Transmission electron microscopy (TEM)

Tissue samples were minced to <0.5 mm^3, fixed in Karnovsky's solution (1% glutaraldehyde and 4% paraformaldehyde in 0.1M phosphate buffer) for 24

hours, and followed by post-fixation in 1% osmium tetroxide. After fixation, all of the samples were dehydrated in series graded ethanol solutions and embedded in an Epon-epoxy mixture. Ultra-thin 70 nm thick sections were prepared by using Leica Ultracut 7 for TEM according to standard procedures. The sections were then examined by an electron microscope (Tecnai Spirit, FEI) operated at 80 kV. An AMT camera system was used for electron microscopy and image capture. The quantity and diameter of EVs were analyzed using ImageJ software.

Statistics

The paired samples t-tests were performed to evaluate the statistical differences of protein expression levels, EV numbers and sizes between PWS lesions and normal controls. Data presented as "mean ± S.D." and $p<0.05$ were considered significant.

Results

A total of 299 proteins from PWS FFPE samples were identified by SWATH-MS, among which 107 showed significant changes in their expression levels in PWS lesions as compared to normal skin (Table 1). Metabolism/biosynthesis, cytoskeleton, cell adhesion/ connective tissue and membrane trafficking were the leading functional categories of these DE proteins, accounting for 24.7%, 20.9%, 11.9% and 10.9% of total 107 DE proteins, respectively (Fig. 1A).

We then performed an immunoblot assay to verify the expression levels of some key molecules with functions related to cell membrane trafficking/ exocytosis, including IQGAP1, VAT1, spectrin 1α, clathrin, GDIR1, HSC70 and perlecan. We found that the expression levels of all of these proteins showed a significant increase in PWS hypertrophic lesions and nodules as compared to control (Figs. 1B,C). In addition, we confirmed that the expression of VDBP was significantly higher in PWS hypertrophic lesions and nodules as compared to control. The expressions of Col6A1, Col6A3 and Anx1 showed significant decreases in PWS lesions as compared to control (Fig. 1B,C). These results were consistent with our SWATH-MS data (Table 1).

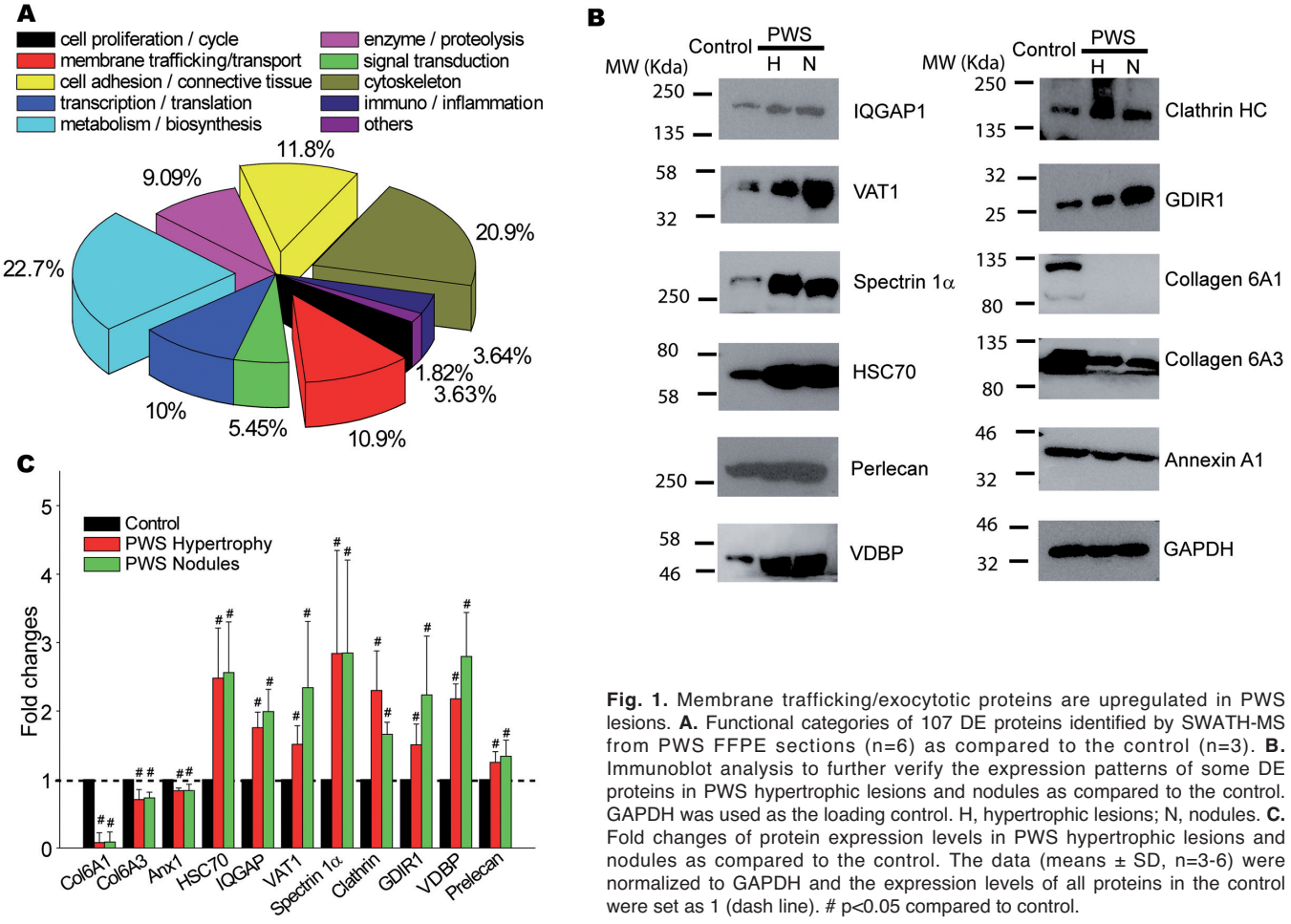

Fig. 1. Membrane trafficking/exocytotic proteins are upregulated in PWS lesions. **A.** Functional categories of 107 DE proteins identified by SWATH-MS from PWS FFPE sections (n=6) as compared to the control (n=3). **B.** Immunoblot analysis to further verify the expression patterns of some DE proteins in PWS hypertrophic lesions and nodules as compared to the control. GAPDH was used as the loading control. H, hypertrophic lesions; N, nodules. **C.** Fold changes of protein expression levels in PWS hypertrophic lesions and nodules as compared to the control. The data (means ± SD, n=3-6) were normalized to GAPDH and the expression levels of all proteins in the control were set as 1 (dash line). # $p<0.05$ compared to control.

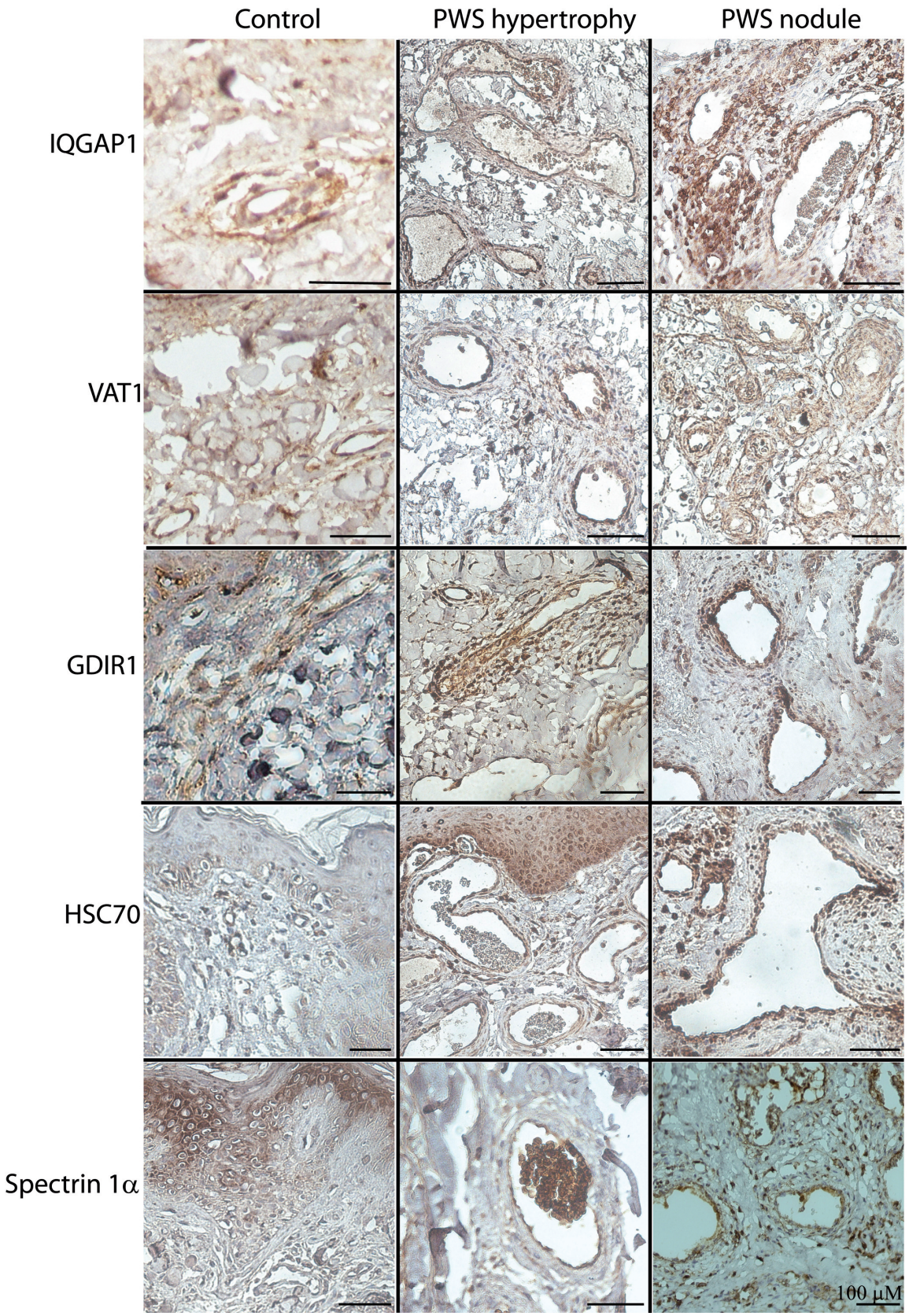

Fig. 2. Immunohistochemical localization of increased IQGAP1, VAT1, GDIR1, HSC70 and spectrin 1α proteins in blood vessels of PWS hypertrophic lesions and nodules as compared to normal skin control. Scale bar: 100 μM.

We next attempted to determine the cellular localization of IQGAP1, VAT1, GDIR1, HSC70 and spectrin 1α in PWS lesions by IHC. IQGAP1, VAT1, GDIR1, HSC70 and Spectrin 1α showed a negative or mild expression in normal dermal blood vessels (Fig. 2). In PWS hypertrophic lesions and nodules, all of these proteins were evidently expressed in endothelial cells (ECs). IQGAP1, VAT1, GDIR1 and HSC70 also showed a strong immuno-reactive (IR) signal in pericytes and some fibroblasts (Fig. 2). In PWS nodules, the synaptic protein VAT1 expression extended throughout the entire PWS blood vessel stroma, showing a membrane pattern (Fig. 2).

The upregulation of a variety of membrane trafficking related proteins in PWS lesions led us to posit that PWS ECs may aberrantly secrete EVs. We then performed TEM studies to examine the fine structures of PWS as compared to normal dermal vessels. We observed a large number of EVs actively budding off from the PWS vessel wall into the lumen in both infantile and adult PWSs (Figs. 3A-C). The quantity of EVs released from PWS blood vessel ECs showed a significant increase by 2.8- fold as compared to control vessels (1.4107±0.6309 vs 0.3196±0.2384 per unit length (μm) of endothelium, p=0.0152, n=6 subjects) (Fig. 3D). Furthermore, the average diameter of EVs released from PWS is slightly, but significantly larger, than control vessels (0.3494±0.1495 vs 0.30118±0.1793

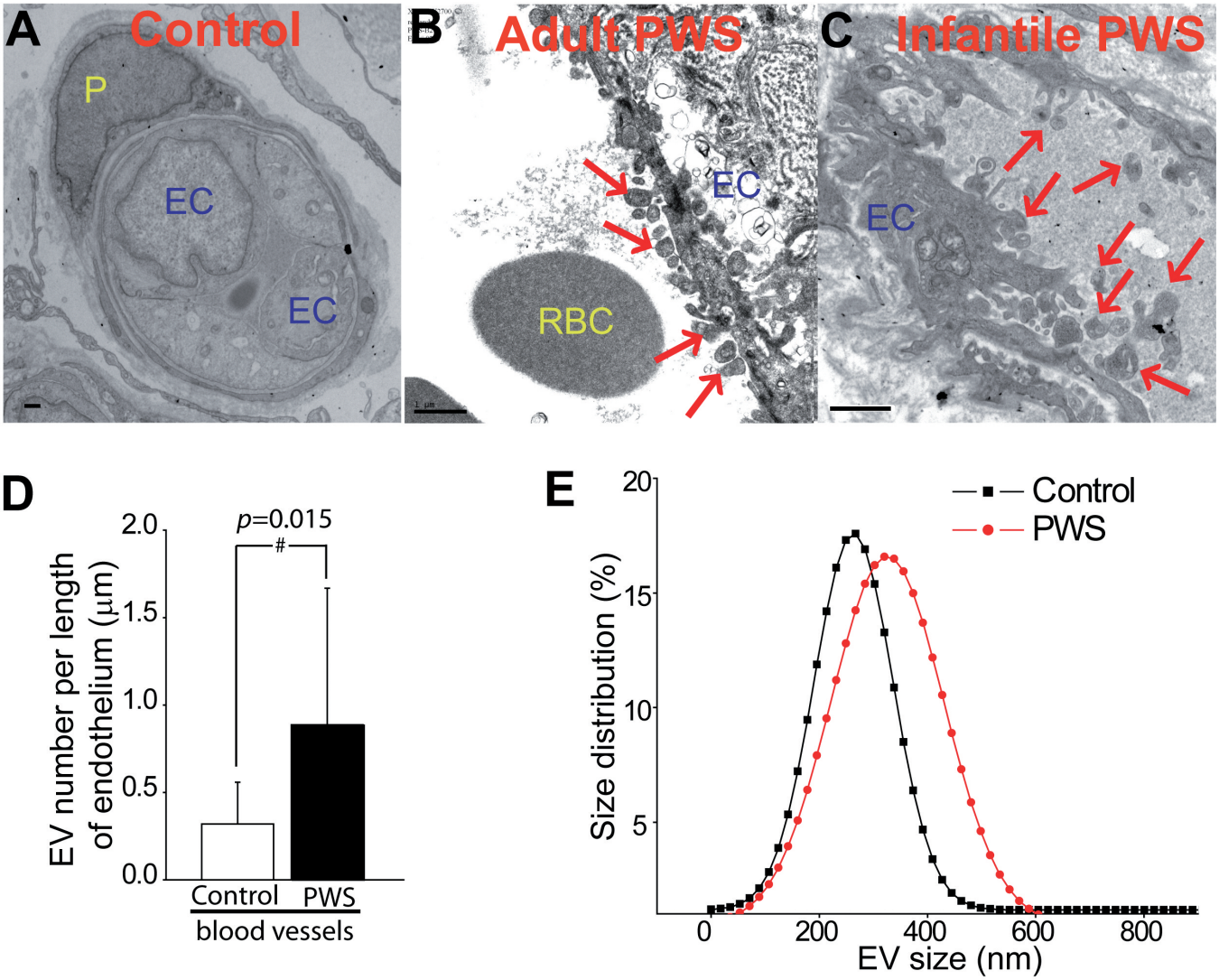

Fig. 3. TEM showing an enhancement of EVs exocytosis in PWS blood vessels as compared to normal skin. **A.** normal ECs. EVs (red arrows) were released from an adult PWS EC **(B)**, and an infantile PWS EC blood vessel **(C).** P, pericyte; RBC, red blood cell; EC, endothelial cell. **D.** Quantitative analysis of the number of released EVs from PWS ECs as compared to control (n=6 subjects). **E.** Size distribution of released EVs from PWS ECs as compared to control (n=6 subjects). Scale bar: 1 μm.

μm, p=0.0472, n=6 subjects) (Fig. 3E). These findings suggest that PWS blood vessel ECs actively secrete more and larger EVs as compared to controls, demonstrating the aberrant upregulation of exocytosis pathways in PWS blood vessels.

Discussion

In this study, we have identified 107 DE proteins from FFPE PWS tissues as compared to normal skin, which are mainly involved in the functional processes of metabolism/biosynthesis, membrane trafficking, cytoskeleton and cell adhesion/migration. These results are consistent with our recent TEM study showing that PWS ECs, pericytes, and fibroblasts are very hyperactive in biosynthesis, metabolism and vesicular secretion (Gao et al., 2017). We further confirmed that the expressions of membrane trafficking/exocytosis related proteins, including VAT1, IQGAP1, HSC70, clathrin, perlecan, spectrin 1α and GDIR1, are significantly upregulated in PWS blood vessels in both hypertrophic lesions and nodules. The aberrant expression patterns of these proteins may underlie the molecular mechanism of the enhanced secretion of EVs from PWS blood vessels that was observed in our TEM study. Furthermore, we have identified that levels of Col6A1 and Col6A3 proteins are decreased in in PWS lesions, which provide initial steps to determine the mechanism accounting for the collagenous alterations that we previously reported from infantile up through hypertrophic lesions and nodules (Tan et al., 2016a,b; Gao et al., 2017).

Table 1. List of SWATH-MS-identified proteins and DE candidates from FFPE PWS samples.

Protein	Protein ID	Changes	T-test p value	Protein full name
CALM	P62158	decrease	0.0000	Calmodulin
ANXA1	P04083	decrease	0.0378	Annexin I
MIME	P20774	decrease	0.0059	Mimecan
DERM	Q07507	decrease	0.0034	Dermatopontin
PPIA	P62937	decrease	0.0031	Peptidyl-prolyl cis-trans isomerase A
ANXA5	P08758	decrease	0.0100	Annexin 5
SUCB2	Q96I99-2	decrease	0.0449	GTP-specific succinyl-CoA synthetase subunit beta, isoform 2
CO4A	P0C0L4	decrease	0.0001	Complement C4-A
TBB4B	P68371	decrease	0.0002	Tubulin beta-4B
COX2	P00403	decrease	0.0092	Cytochrome c oxidase, Subunit 2
CO6A3	P12111-2	decrease	0.0194	Collagen 6 A3
TBA1B	P68363	decrease	0.0065	Tubulin beta-1B
ENOA	P06733	decrease	0.0018	alpha-enloase
KPYM	P14618-3	decrease	0.0029	Pyruvate kinase PKM
ATPB	P06576	decrease	0.0286	ATP synthase subunit beta, mitochondrial
KV201	P01614	decrease	0.0066	Immunoglobulin kappa variable 2D-40
ACTBL	Q562R1	decrease	0.0044	Beta-actin-like protein 2
CO6A1	P12109	decrease	0.0338	Collagen alpha-1(VI) chain
PRELP	P51888	decrease	0.0036	Prolargin
IGHG1	P01857	decrease	0.0120	Immunoglobulin heavy constant gamma 1
THIO	P10599	decrease	0.0103	Thioredoxin
TBB5	P07437	decrease	0.0228	Tubulin beta chain
PGK1	P00558	decrease	0.0306	Phosphoglycerate kinase 1
ACTBM	Q9BYX7	decrease	0.1050	Putative beta-actin-like protein 3
LUM	P51884	decrease	0.0003	Lumican
POTEF	A5A3E0	decrease	0.0100	POTE ankyrin domain family member F
LAC7	A0M8Q6	decrease	0.0850	Immunoglobulin lambda constant 7
TBA4A	P68366	decrease	0.0030	Tubulin alpha-4A chain
APOA1	P02647	decrease	0.0151	Apolipoprotein A-I
CBPA3	P15088	decrease	0.0068	Mast cell carboxypeptidase A
PGS2	P07585	decrease	0.0377	Decorin
CMA1	P23946	decrease	0.0971	Chymase
DSG1	Q02413	decrease	0.0321	Desmoglein-1
TRYB2	P20231	decrease	0.0348	Tryptase beta-2
LDHA	P00338-3	decrease	0.0393	L-lactate dehydrogenase A chain
HSP71	P08107	decrease	0.0274	Heat shock 70 kDa protein 1
TPIS	P60174-1	decrease	0.0164	Triosephosphate isomerase
POSTN	Q15063-3	decrease	0.0219	Periostin
POTEJ	P0CG39	decrease	0.0135	POTE ankyrin domain family member J
LEG3	P17931	decrease	0.0209	Galectin-3
HSPB1	P04792	decrease	0.0368	Heat shock protein beta-1
RLA2	P05387	decrease	0.0379	60S acidic ribosomal protein P2
PRDX6	P30041	decrease	0.0448	Peroxiredoxin-6

Table 1. (Continuation).

Protein	Protein ID	Changes	T-test p value	Protein full name
CACP	P43155-2	increase	0.0144	Carnitine O-acetyltransferase
ML12B	O14950	increase	0.0005	Myosin regulatory light chain 12B
E9PBV3	Q6UWP8	increase	0.0005	Suprabasin
K1C9	P35527	increase	0.0139	Keratin, type I cytoskeletal 9
UBA1	P22314	increase	0.0002	Ubiquitin-like modifier-activating enzyme 1
K2C6B	P04259	increase	0.0082	Keratin, type II cytoskeletal 6B
IMB1	Q14974	increase	0.0107	Importin subunit beta-1
CAN1	P07384	increase	0.0636	Calpain-1 catalytic subunit
Septin-7	Q16181-2	increase	0.0012	Septin-7
NPM	P06748-2	increase	0.0378	Nucleophosmin
FACR2	Q96K12	increase	0.0192	Fatty acyl-CoA reductase 2
FBLN2	P98095-2	increase	0.0183	Fibulin-2
NDUAD	Q9P0J0	increase	0.0029	NADH dehydrogenase 1 alpha subcomplex subunit 13
VAT1	Q99536	increase	0.0212	Synaptic vesicle membrane protein VAT-1 homolog
HNRPU	Q00839-2	increase	0.0073	Heterogeneous nuclear ribonucleoprotein U
ADT3	P12236	increase	0.0566	ADP/ATP translocase 3
RL13A	P40429	increase	0.0028	60S ribosomal protein L13a
ACADV	P49748-2	increase	0.0003	Very long-chain specific acyl-CoA dehydrogenase
G6PI	P06744-2	increase	0.0878	Glucose-6-phosphate isomerase
PLEC	Q15149-2	increase	0.0222	Plectin-1
HNRPC	P07910-2	increase	0.0299	Heterogeneous nuclear ribonucleoproteins C1/C2
AL3A2	P51648-2	increase	0.0065	Fatty aldehyde dehydrogenase 2
IF5A1	P63241-2	increase	0.0070	Eukaryotic translation initiation factor 5A-1
GDIR1	P52565	increase	0.0195	Rho GDP-dissociation inhibitor 1
VTDB	P02774-2	increase	0.0004	Vitamin D-binding protein
TKT	P29401	increase	0.0007	Transketolase
TCPB	P78371	increase	0.0074	T-complex protein 1 subunit beta
C1QBP	Q07021	increase	0.0162	Complement component 1 Q subcomponent-binding protein
K2C3	P12035	increase	0.0241	Keratin, type II cytoskeletal 3
CAPZB	P47756-2	increase	0.0027	F-actin-capping protein subunit beta
GANAB	Q14697-2	increase	0.0320	Neutral alpha-glucosidase AB
ANXA6	P08133	increase	0.0224	Annexin A6
PTBP1	P26599-2	increase	0.0509	Polypyrimidine tract-binding protein 1
K2C1B	Q7Z794	increase	0.0650	Keratin, type II cytoskeletal 1b
F16P1	P09467	increase	0.0071	Fructose-1,6-bisphosphatase 1
CNDP2	Q96KP4	increase	0.0134	Cytosolic non-specific dipeptidase
MOES	P26038	increase	0.0054	Moesin
CYB5	P00167	increase	0.0154	Cytochrome b5
PRDBP	Q969G5	increase	0.0392	Caveolae-associated protein 3
EHD2	Q9NZN4	increase	0.0011	EH domain-containing protein 2
PHB	P35232	increase	0.0160	Prohibitin
CDC42	P60953	increase	0.0017	Cell division control protein 42 homolog
RTN3	O95197-2	increase	0.0042	Reticulon-3
CISY	O75390	increase	0.0158	Citrate synthase, mitochondrial
SPTBN1	Q01082	increase	0.0459	Spectrin, non-erythrocytic 1
HEP2	P05546	increase	0.0056	Heparin cofactor 2
ACOC	P21399	increase	0.0041	Cytoplasmic aconitate hydratase
CD44	P16070-10	increase	0.0366	CD44 antigen
CLH1	Q00610-2	increase	0.0069	Clathrin heavy chain 1
CALL5	Q9NZT1	increase	0.0554	Calmodulin-like protein 5
IQGA1	P46940	increase	0.0030	Ras GTPase-activating-like protein IQGAP1
ECHA	P40939	increase	0.0009	Trifunctional enzyme subunit alpha
MYO1C	O00159-2	increase	0.0434	Unconventional myosin-Ic
HSC70	P11142	increase	0.0035	Heat shock cognate 71 kDa protein
TRY6	Q8NHM4	increase	0.0404	Putative trypsin-6
ANXA7	P20073-2	increase	0.0290	Annexin A7
ASPN	Q9BXN1	increase	0.0299	Asporin
U2AF1	Q01081-2	increase	0.0153	Splicing factor U2AF 35 kDa subunit
FIBB	P02675	increase	0.0416	Fibrinogen beta chain
PGAM2	P15259	increase	0.0171	Phosphoglycerate mutase 2
CAP1	Q01518-2	increase	0.0141	Adenylyl cyclase-associated protein 1
SERPH	P50454	increase	0.0377	Serpin H1
RL36	Q9Y3U8	increase	0.0203	60S ribosomal protein L36
RS12	P25398	increase	0.0030	40S ribosomal protein S12

Table 1. (Continuation).

Protein	Protein ID	Changes	T-test p value	Protein full name
K2C1	P04264		0.1139	Keratin, type II cytoskeletal 1
ACTG	P63261		0.1772	Actin, cytoplasmic 2
ATPA	P25705		0.1091	ATP synthase subunit alpha, mitochondrial
SODM	P04179		0.2067	Superoxide dismutase [Mn], mitochondrial
K1C10	P13645		0.2558	Keratin, type I cytoskeletal 10
K22E	P35908		0.1209	Keratin, type II cytoskeletal 2 epidermal
BLMH	Q13867		0.2180	Bleomycin hydrolase
DHE3	P00367		0.1715	Glutamate dehydrogenase 1, mitochondrial
NDK8	O60361		0.1076	Putative nucleoside diphosphate kinase
EPIPL	P58107		0.0836	Epiplakin
CO1A2	P08123		0.3556	Collagen alpha-2(I) chain (Alpha-2 type I collagen)
MYH11	P35749-2		0.0528	Myosin-11
TTHY	P02766		0.3882	Transthyretin
K2C6C	P48668		0.7864	Keratin, type II cytoskeletal 6C
ACOT1	Q86TX2		0.1130	Acyl-coenzyme A thioesterase 1
H2B1J	P06899		0.2799	Histone H2B type 1-J
HS90B	P08238		0.2158	Heat shock protein HSP 90-beta
CO1A1	P02452		0.3156	Collagen alpha-1(I) chain
CALX	P27824		0.1385	Calnexin
APMAP	Q9HDC9-2		0.2214	Adipocyte plasma membrane-associated protein
MDHC	P40925-2		0.8702	Malate dehydrogenase, cytoplasmic
RTN4	Q9NQC3-2		0.6569	Reticulon-4
ACLY	P53396-2		0.2295	ATP-citrate synthase
K2C79	Q5XKE5		0.1895	Keratin, type II cytoskeletal 79
OLFL1	Q6UWY5		0.2413	Olfactomedin-like protein 1
DESM	P17661		0.6252	Desmin
PDIA1	P07237		0.0617	Protein disulfide-isomerase
CALL3	P27482		0.8993	Calmodulin-like protein 3
IGKC	P01834		0.2819	Immunoglobulin kappa constant
RS3	P23396		0.5846	40S ribosomal protein S3
GRP75	P38646		0.4332	Stress-70 protein, mitochondrial
SPTN1	Q13813-2		0.1086	Spectrin alpha chain, non-erythrocytic 1
HS90A	P07900-2		0.2423	Heat shock protein HSP 90-alpha
MDHM	P40926		0.1712	Malate dehydrogenase, mitochondrial
1433G	P61981		0.1608	14-3-3 protein gamma
KCRU	P12532		0.3709	Creatine kinase U-type, mitochondrial
MGST1	P10620		0.4115	Microsomal glutathione S-transferase 1
PLST	P13797		0.3280	Plastin-3
TENX	P22105-3		0.3180	Tenascin-X
GSTP1	P09211		0.7356	Glutathione S-transferase P
SPB5	P36952-2		0.7185	Serpin B5
K1C17	Q04695		0.4547	Keratin, type I cytoskeletal 17
CH10	P61604		0.7309	10 kDa heat shock protein, mitochondrial
K2C5	P13647		0.9602	Keratin, type II cytoskeletal 5
K2C75	O95678		0.7730	Keratin, type II cytoskeletal 75
KRHB4	Q9NSB2		0.2100	Keratin, type II cuticular Hb4
ACSL1	P33121-2		0.2422	Long-chain-fatty-acid--CoA ligase 1
PEBP1	P30086		0.1779	Phosphatidylethanolamine-binding protein 1
CH60	P10809		0.2522	60 kDa heat shock protein, mitochondrial
EF2	P13639		0.8619	Elongation factor 2
G3P	P04406		0.1730	Glyceraldehyde-3-phosphate dehydrogenase
ROA2	P22626-2		0.0821	Heterogeneous nuclear ribonucleoproteins A2/B1
SAMP	P02743		0.5089	Serum amyloid P-component
ACTN4	O43707		0.1769	Alpha-actinin-4
CO7A1	Q02388-2		0.3306	Collagen alpha-1(VII) chain
ANXA2	P07355		0.0670	Annexin A2
TPM4	P67936		0.8825	Tropomyosin alpha-4 chain
K2C7	P08729		0.1376	Keratin, type II cytoskeletal 7
TAGL2	P37802		0.6384	Transgelin-2
TAGL	Q01995		0.9556	Transgelin
DESP	P15924		0.8624	Desmoplakin
KRHB1	Q14533		0.6614	Keratin, type II cuticular Hb1
ATPD	P30049		0.9944	ATP synthase subunit delta, mitochondrial
H13	P16402		0.7264	Histone H1.3
PKP1	Q13835-2		0.4539	Plakophilin-1
Q6ZN40	Q6ZN40		0.7311	Tropomyosin 1 (Alpha), isoform CRA_f
VINC	P18206-2		0.3318	Vinculin

Table 1. (Continuation).

Protein	Protein ID	Changes	T-test p value	Protein full name
TPM3	P06753-2		0.9364	Tropomyosin alpha-3 chain
MYH9	P35579		0.6876	Myosin-9
QCR2	P22695		0.0904	Cytochrome b-c1 complex subunit 2, mitochondrial
HMCS1	Q01581		0.1303	Hydroxymethylglutaryl-CoA synthase, cytoplasmic
PTRF	Q6NZI2		0.1133	Caveolae-associated protein 1
KRT34	AOA140TA69		0.5223	Keratin, type I cuticular 34
FIBG	P02679-2		0.5412	Fibrinogen gamma chain
CBR1	P16152		0.5535	Carbonyl reductase [NADPH] 1
IGHV1-69	P01742		0.3966	Immunoglobulin heavy variable 1-69
AK1A1	P14550		0.3532	Alcohol dehydrogenase [NADP(+)]
RS7	P62081		0.0898	40S ribosomal protein S7
6PGD	P52209		0.1932	6-phosphogluconate dehydrogenase, decarboxylating
K1HB	Q14525		0.7606	Keratin, type I cuticular Ha3-II
RINI	P13489		0.4873	Ribonuclease inhibitor
KRHB5	P78386		0.3782	Keratin, type II cuticular Hb5
ACTA	P62736		0.3669	Actin, aortic smooth muscle
1433T	P27348		0.5399	14-3-3 protein theta
1433S	P31947-2		0.1912	14-3-3 protein sigma
KT33A	O76009		0.5778	Keratin, type I cuticular Ha3-I
ANXA4	P09525		0.3965	Annexin A4
COF1	P23528		0.1697	Cofilin-1
DCD	P81605-2		0.3436	Dermcidin
MYL6	P60660-2		0.4113	Myosin light polypeptide 6
CO3	P01024		0.3680	Complement C3
ALDOA	P04075		0.7189	Fructose-bisphosphate aldolase A
F8WA83	F8WA83		0.1590	Protein disulfide-isomerase A6
RS25	P62851		0.6396	40S ribosomal protein S25
RLA0	P05388		0.8649	60S acidic ribosomal protein P0
FPPS	P14324		0.6824	Farnesyl pyrophosphate synthase
SODE	P08294		0.7150	Extracellular superoxide dismutase [Cu-Zn]
PDIA3	P30101		0.3960	Protein disulfide-isomerase A3
H2AZ	P0C0S5		0.2815	Histone H2A.Z
CO6A2	P12110		0.07811	Collagen alpha-2(VI) chain
UBB	P0CG47		0.2636	Polyubiquitin-B
H14	P10412		0.7302	Histone H1.4
H12	P16403		0.9632	Histone H1.2
PPIB	P23284		0.0415	Peptidyl-prolyl cis-trans isomerase B
IGHA1	P01876		0.0592	Immunoglobulin heavy constant alpha 1
PRDX2	P32119		0.2307	Peroxiredoxin-2
TETN	P05452		0.6625	Tetranectin
CO2A1	P02458-1		0.7240	Collagen alpha-1(II) chain
PGS1	P21810		0.6091	Biglycan
PLSL	P13796		0.2034	Plastin-2
K1C16	P08779		0.1750	Keratin, type I cytoskeletal 16
TERA	P55072		0.3518	Transitional endoplasmic reticulum ATPase
IF4A1	P60842		0.5670	Eukaryotic initiation factor 4A-I
ALDH2	P05091		0.1389	Aldehyde dehydrogenase, mitochondrial
F213A	Q9BRX8-2		0.3071	Redox-regulatory protein FAM213A
TRFE	P02787		0.9619	Serotransferrin
DLDH	P09622		0.1199	Dihydrolipoyl dehydrogenase, mitochondrial
HBA	P69905		0.6317	Hemoglobin subunit alpha
ADT2	P05141		0.1362	ADP/ATP translocase 2
S10A4	P26447		0.2537	Protein S100-A4
K2C6A	P02538		0.7811	Keratin, type II cytoskeletal 6A
K2C71	Q3SY84		0.3118	Keratin, type II cytoskeletal 71
FIBA	P02671-2		0.8840	Fibrinogen alpha chain
RAB1A	P62820		0.1385	Ras-related protein Rab-1A
PRDX3	P30048		0.5286	Thioredoxin-dependent peroxide reductase
HNRPM	P52272-2		0.1103	Heterogeneous nuclear ribonucleoprotein M
COEA1	Q05707-2		0.1047	Collagen alpha-1(XIV) chain
CATD	P54720		0.5173	Putative oxidoreductase CatD
CYTB	P04080		0.2558	Cystatin-B
HBD	P02042		0.8510	Hemoglobin subunit delta
COCA1	Q99715-4		0.2653	Collagen alpha-1(XII) chain
PARK7	Q99497		0.5698	Protein DJ-1

Table 1. (Continuation).

Protein	Protein ID	Changes	T-test p value	Protein full name
HBB	P68871		0.7369	Hemoglobin subunit beta
H4	P62805		0.5921	Histone H4
PLAK	P14923		0.0868	Junction plakoglobin
FADS2	O95864-3		0.2638	Fatty acid desaturase 2
VIME	P08670		0.2791	Vimentin
GDIB	P50395		0.4545	Rab GDP dissociation inhibitor beta
AMBP	P02760		0.2800	Protein AMBP
ACADM	P11310-2		0.1668	Medium-chain specific acyl-CoA dehydrogenase
AHNK	Q09666		0.2044	Neuroblast differentiation-associated protein AHNAK
RL11	P62913-2		0.5031	60S ribosomal protein L11
BLVRB	P30043		0.9121	Flavin reductase (NADPH)
1433B	P31946-2		0.1837	14-3-3 protein beta/alpha
LEG7	P47929		0.2234	Galectin-7
LX15B	O15296-3		0.9051	Arachidonate 15-lipoxygenase B
E7EN67	UPI0000D623EA		0.2188	
RSSA	P08865		0.2774	40S ribosomal protein SA
H2B1K	O60814		0.2670	Histone H2B type 1-K
PRDX1	Q06830		0.3174	Peroxiredoxin-1
GRP78	P11021		0.1801	78 kDa glucose-regulated protein
F13A	P00488		0.4218	Coagulation factor XIII A chain
ACTN1	P12814-2		0.5855	Alpha-actinin-1
A1AT	P01009-2		0.3595	Alpha-1-antitrypsin
ALBU	P02768		0.6580	Serum albumin
CO3A1	P02461		0.8563	Collagen alpha-1(III) chain
PLIN3	O60664-3		0.1000	Perilipin-3
HV305	P01766		0.0699	Immunoglobulin heavy variable 3-13
1433E	P62258-2		0.1358	14-3-3 protein epsilon
DEST	P60981-2		0.7139	Destrin
SERA	O43175		0.0964	D-3-phosphoglycerate dehydrogenase
PYGB	P11216		0.5287	Glycogen phosphorylase, brain form
FLNA	P21333-2		0.1114	Filamin-A
KCD12	Q96CX2		0.0769	BTB/POZ domain-containing protein KCTD12
ENPL	P14625		0.1996	Endoplasmin
HEMO	P02790		0.9227	Hemopexin
K1C14	P02533		0.2896	Keratin, type I cytoskeletal 14
K2C8	P05787		0.1272	Keratin, type II cytoskeletal 8
FAS	P49327		0.0829	Fatty acid synthase
RAB7A	P51149		0.7764	Ras-related protein Rab-7a
K1C15	P19012		0.5779	Keratin, type I cytoskeletal 15
TBAL3	A6NHL2-2		0.9280	Tubulin alpha chain-like 3
ANXA4	P09525		0.3780	Annexin A4
H10	P07305-2		0.5124	Histone H1.0
H2A1B	P04908		0.2242	Histone H2A type 1-B/E
GELS	P06396		0.2569	Gelsolin
EF1A1	P68104		0.1503	Elongation factor 1-alpha 1
GLRX1	P35754		0.7463	Glutaredoxin-1
IDHP	P48735		0.1151	Isocitrate dehydrogenase [NADP], mitochondrial
HNRPK	P61978-2		0.8073	Heterogeneous nuclear ribonucleoprotein K
K1C19	P08727		0.6558	Keratin, type I cytoskeletal 19
AL9A1	P49189		0.6336	4-trimethylaminobutyraldehyde dehydrogenase
CLIC1	O00299		0.5148	Chloride intracellular channel protein 1
DPYL2	Q16555		0.74210	Dihydropyrimidinase-related protein 2
AN32A	P39687		0.3995	Acidic leucine-rich nuclear phosphoprotein 32 family member A
LMNA	P02545		0.2599	Prelamin-A/C
PROF1	P07737		0.1528	Profilin-1
1433Z	P63104		0.1740	14-3-3 protein zeta/delta
RL22	P35268		0.8040	60S ribosomal protein L22
K1H1	Q15323		0.7391	Keratin, type I cuticular Ha1
F5GWP8	F5GWP8		0.6802	Keratin, type I cytoskeletal 17
BGH3	Q15582		0.2281	Transforming growth factor-beta-induced protein Ig-h3

Biosynthesis and exocytosis of EVs is a biological process that consists of vesicular membrane trafficking and fusion of intracellular vesicles with the plasma membrane for secretion. The EVs contain cell type-specific compositions of cellular contents such as lipids, proteins, mRNAs and microRNAs. EVs can be taken up by a variety of neighboring cells and by systemic circulation into distant cells; thus, EVs can facilitate intercellular communications by exchanging biological contents among cells (Denzer et al., 2000; Simons and Raposo, 2009; Record et al., 2011; Ludwig and Giebel, 2012). Vesicular membrane trafficking requires dynamic rearrangements of the intracellular cytoskeleton architecture. Many proteins can function as key regulators for cytoskeleton remodeling, such as IQGAP1, clathrin, spectrin 1α, HSC70, calmodulin (CaM) and GDIR1, to modulate EV membrane trafficking. These proteins either interact with the cytoskeleton as it scaffolds to recruit their partner proteins or act as modulators to regulate cytoskeleton reorganization. For example, IQGAP1 has been shown to play multiple roles at different steps in the membrane trafficking/exocytosis by: (1) linking to actin via S100 in a Ca^{2+}-dependent manner, which can be regulated by CaM; (2) regulating actin dynamics to facilitate vesicle docking and fusion with the plasma membrane; (3) interacting with CDC42 and regulating the exocytosis in gastric parietal cells and epithelial cells; (4) forming a complex with Rab27A and regulating exocytosis of insulin-containing vesicles in pancreatic β cells; and (5) associating with exocyst complex molecules, such as Exo70, Sec3 and Sec8, which mediate the tethering of exocytotic vesicles (Noordstra and Akhmanova, 2017). HSC70 forms a complex with other co-chaperones and enhances the chaperone's ATPase activity, thus regulating vesicle exocytosis and endocytosis (Gorenberg and Chandra, 2017). Clathrin is one of the major proteins involved in the formation of coated vesicles. VAT1, spectrin 1α and clathrin have been found in synaptic protein complexes (Phillips et al., 2001; Lohoff, 2010). In this study, we have shown that all of these proteins are dysregulated in PWS lesions (Fig. 1, Table 1), suggesting an aberrant alteration in EV formation and exocytosis in PWS lesions. Indeed, our TEM studies have further confirmed that PWS ECs release more EVs than normal ECs. These findings together suggest that upregulation of membrane trafficking/exocytotic proteins results in enhanced EV biosynthesis and release from PWS ECs. These EVs contain specific cell tropism from the parental lesional ECs where they are produced and released which can orchestrate the essential pathological signaling into neighboring ECs and pericytes, causing disease progression. It can be speculated that these EVs may be released into the circulation where they can be isolated and their EC-specific compositions can be characterized to identify the unique pathological phenotypes of PWS blood vessels. However, it is unclear how these upregulated membrane trafficking/exocytotic proteins regulate EV biosynthesis and release and whether they are to be transported outside the parental cell membranes along with EVs. A series of immuno-TEM studies using specific antibodies will be required to further dissect the mechanistic basis of the aberrant EV exocytosis in PWS lesions, which will be the next focus in our study. Furthermore, the function of these EVs in the pathogenesis of PWS remains to be determined in future studies.

In addition, upregulation of IQGAP1, perlecan and spectrin may modulate cell adhesion/mobility signaling, thus contributing to the progressive dilatation of PWS blood vessels, the most prominent clinical phenotype of the disease. IQGAP1 can crosslink actin filaments *via* its calponin homology domain or interact with a subset of microtubule associated proteins to facilitate cell mobility (Watanabe et al., 2015; Noordstra and Akhmanova, 2017). Spectrin can interact with annx family members, such as annx 6, to modulate proteolysis for adhesion complexes, including focal adhesion kinase (FAK) (Grewal et al., 2017). In addition, perlecan regulates angiogenesis and facilitates migration of ECs (Nakamura et al., 2015). In this study, the expressions of IQGAP1, perlecan, and spectrin are upregulated in PWS ECs. Our data suggest that enhanced expression of these molecules may contribute to the steady and dynamic expansion of PWS ECs over time. In particular, the upregulation of IQGAP1 is also found in pericytes and fibroblasts in PWS lesions, suggesting its potential roles in mediating the progressive expansion of the entire PWS blood vessel into matrix of the dermis as well as outgrowth of the soft tissues seen in hypertrophic lesions and nodules.

The present study shows that multiple proteins involving membrane trafficking and exocytosis are upregulated in PWS lesions in association with an enhancement of secretion of EVs from PWS blood vessels, providing a fundamental database for further studies to evaluate the roles of these DE proteins and EC EVs-mediated signaling pathways in the pathogenesis of PWS.

Acknowledgements. Institutional support was provided by the Arnold and Mabel Beckman Foundation and the David and Lucile Packard Foundation. We greatly appreciate the Sue & Bill Gross Stem Cell Research Center at the University of California, Irvine, for their assistance with the histology image acquisition process experiments.

Conflict of Interest. Disclosure: None Declared

Disclaimer. Any views expressed here represent personal opinion and do not necessarily reflect those of the United States Department of Health and Human Services or the federal government.

Prior Publication. None of the material in this manuscript has been published or is under consideration for publication elsewhere, including the Internet.

Funding statement. This work was supported by grants from the National Institutes of Health (AR063766 and AR073172 to WT, HL70562 to DBC, AR47551 and AR59244 to JSN), the Department of Defense/CDMRP (W81XWH1810096 to WT) and National Natural Science Foundation of China (81571432 to YT).

References

Couto J.A., Huang L., Vivero M.P., Kamitaki N., Maclellan R.A., Mulliken J.B., Bischoff J., Warman M.L. and Greene A.K. (2016). Endothelial cells from capillary malformations are enriched for somatic gnaq mutations. Plast. Reconstr. Surg. 137, 77e-82e.

Denzer K., Kleijmeer M.J., Heijnen H.F., Stoorvogel W. and Geuze H.J. (2000). Exosome: From internal vesicle of the multivesicular body to intercellular signaling device. J. Cell Sci. 113 Pt 19, 3365-3374.

Deutsch E.W., Shteynberg D., Lam H., Sun Z., Eng J.K., Carapito C., von Haller P.D., Tasman N., Mendoza L., Farrah T. and Aebersold R. (2010). Trans-proteomic pipeline supports and improves analysis of electron transfer dissociation data sets. Proteomics 10, 1190-1195.

Gao L., Yin R., Wang H., Guo W., Song W., Nelson J.S., Tan W. and Wang G. (2017). Ultrastructural characterization of hyperactive endothelial cells, pericytes and fibroblasts in hypertrophic and nodular port wine stain lesions. Br. J. Dermatol. 177, e105-e108.

Gao L., Phan S., Nadora D.M., Chernova M., Sun V., Preciado S.M., Ballew B., Jia Z., Jia W., Wang G., Mihm M.C. Jr, Nelson J.S. and Tan W. (2014). Topical rapamycin systematically suppresses the early stages of pulsed dye laser-induced angiogenesis pathways. Lasers Surg. Med. 46, 679-688.

Geronemus R.G. and Ashinoff R. (1991). The medical necessity of evaluation and treatment of port-wine stains. J. Dermatol. Surg. Oncol. 17, 76-79.

Gorenberg E.L. and Chandra S.S. (2017). The role of co-chaperones in synaptic proteostasis and neurodegenerative disease. Front. Neurosci. 11, 248.

Grewal T., Hoque M., Conway J.R.W., Reverter M., Wahba M., Beevi S.S., Timpson P., Enrich C. and Rentero C. (2017). Annexin a6-a multifunctional scaffold in cell motility. Cell Adh. Migr. 11, 288-304.

Heller A., Rafman S., Zvagulis I. and Pless I.B. (1985). Birth-defects and psychosocial adjustment. Am. J. Dis. Child. 139, 257-263.

Jacobs A.H. and Walton R.G. (1976). The incidence of birthmarks in the neonate. Pediatrics 58, 218-222.

Kalick S.M. (1978). Toward an interdisciplinary psychology of appearances. Psychiatry 41, 243-253.

Lever W.F. and Schaumburg-Lever G. (1990). Histopathology of the skin, 7th ed. J.B. Lippincott Co. Philadelphia, PA.

Lian C.G., Sholl L.M., Zakka L.R., O T.M., Liu C., Xu S., Stanek E., Garcia E., Jia Y., MacConaill L.E., Murphy G.F., Waner M. and Mihm M.C. Jr (2014). Novel genetic mutations in a sporadic port-wine stain. JAMA Dermatol. 150, 1336-1340.

Lohoff F.W. (2010). Genetic variants in the vesicular monoamine transporter 1 (vmat1/slc18a1) and neuropsychiatric disorders. Methods Mol. Biol. 637, 165-180.

Ludwig A.K. and Giebel B. (2012). Exosomes: Small vesicles participating in intercellular communication. Int. J. Biochem. Cell Biol. 44, 11-15.

Malm M. and Carlberg M. (1988). Port-wine stain - a surgical and psychological problem. Ann. Plast. Surg. 20, 512-516.

Nakamura R., Nakamura F. and Fukunaga S. (2015). Perlecan diversely regulates the migration and proliferation of distinct cell types in vitro. Cells Tissues Organs 200, 374-393.

Noordstra I. and Akhmanova A. (2017). Linking cortical microtubule attachment and exocytosis. F1000Res 6, 469.

Ostasiewicz P., Zielinska D.F., Mann M. and Wisniewski J.R. (2010). Proteome, phosphoproteome, and N-glycoproteome are quantitatively preserved in formalin-fixed paraffin-embedded tissue and analyzable by high-resolution mass spectrometry. J. Proteome. Res. 9, 3688-3700.

Phillips G.R., Huang J.K., Wang Y., Tanaka H., Shapiro L., Zhang W., Shan W.S., Arndt K., Frank M., Gordon R.E., Gawinowicz M.A., Zhao Y. and Colman D.R. (2001). The presynaptic particle web: Ultrastructure, composition, dissolution, and reconstitution. Neuron 32, 63-77.

Pratt A.G. (1953). Birthmarks in infants. Arch. Dermatol. Syphilol. 67, 302-305.

Record M., Subra C., Silvente-Poirot S. and Poirot M. (2011). Exosomes as intercellular signalosomes and pharmacological effectors. Biochem. Pharmacol. 81, 1171-1182.

Shirley M.D., Tang H., Gallione C.J., Baugher J.D., Frelin L.P., Cohen B., North P.E., Marchuk D.A., Comi A.M. and Pevsner J. (2013). Sturge-weber syndrome and port-wine stains caused by somatic mutation in gnaq. N. Engl. J. Med. 368, 1971-1979.

Simons M. and Raposo G. (2009). Exosomes--vesicular carriers for intercellular communication. Curr. Opin. Cell Biol. 21, 575-581.

Tan W., Jia W., Sun V., Mihm M.C. Jr and Nelson J.S. (2012). Topical rapamycin suppresses the angiogenesis pathways induced by pulsed dye laser: Molecular mechanisms of inhibition of regeneration and revascularization of photocoagulated cutaneous blood vessels. Lasers Surg. Med. 44, 796-804.

Tan W., Chernova M., Gao L., Sun V., Liu H., Jia W., Langer S., Wang G., Mihm M.C. Jr and Nelson J.S. (2014). Sustained activation of c-jun n-terminal and extracellular signal-regulated kinases in port-wine stain blood vessels. J. Am. Acad. Dermatol. 71, 964-968.

Tan W., Nadora D.M., Gao L., Wang G., Mihm M.C. Jr and Nelson J.S. (2016a). The somatic gnaq mutation (r183q) is primarily located in port wine stain blood vessels. J. Am. Acad. Dermatol. 74, 380-383.

Tan W., Zakka L.R., Gao L., Wang J., Zhou F., Selig M.K., Sukanthanag A., Wang G., Mihm M.C.J. and Nelson J.S. (2016b). Pathological alterations involve the entire skin physiological milieu in infantile and early childhood port wine stain. Br. J. Dermatol. 177, 293-296.

Tan W., Wang J., Zhou F., Gao L., Rong Y., Liu H., Sukanthanag A., Wang G., Mihm M.C. Jr, Chen D.B. and Nelson J.S. (2017). Coexistence of ephb1 and ephrinb2 in port wine stain endothelial progenitor cells contributes to clinicopathological vasculature dilatation. Br. J. Dermatol. 177, 1601-1611.

Tsou C.C., Avtonomov D., Larsen B., Tucholska M., Choi H., Gingras A.C. and Nesvizhskii A.I. (2015). Dia-umpire: Comprehensive computational framework for data-independent acquisition proteomics. Nat. Methods 12, 258-264, 257 p following 264.

Tyanova S., Temu T., Sinitcyn P., Carlson A., Hein M.Y., Geiger T., Mann M. and Cox J. (2016). The perseus computational platform for comprehensive analysis of (prote)omics data. Nat. Methods 13, 731-740.

Watanabe T., Wang S. and Kaibuchi K. (2015). Iqgaps as key regulators of actin-cytoskeleton dynamics. Cell Struct. Funct. 40, 69-77.

Yin R., Gao L., Tan W., Guo W., Zhao T., Nelson J.S. and Wang G. (2017). Activation of PKCα and PI3K kinases in hypertrophic and nodular port wine stain lesions. Am. J. Dermatopathol. 39, 747-752.

Accepted October 10, 2018